Vierros, Sampsa; Österberg, Monika; Sammalkorpi, Maria

Aggregation response of triglyceride hydrolysis products in cyclohexane and triolein

Published in:
Physical chemistry chemical physics : PCCP

DOI:
10.1039/c8cp05104f

Published: 31/10/2018

Document Version
Peer-reviewed accepted author manuscript, also known as Final accepted manuscript or Post-print

Cite this: DOI: 10.1039/C8CP05104F

Aggregation response of triglyceride hydrolysis products in cyclohexane and triolein†

Sampsa Vierros,[a] Monika Österberg,*[b] and Maria Sammalkorpi*[a]

Here, we examine the aggregation response of a series of triglyceride-based biosurfactants in cyclohexane and triglyceride solvents via all-atom molecular dynamics simulations and supporting experiments. The surfactant aggregation follows in all systems, with only minor deviations, a multiple equilibrium, i.e. open association, model. Monoglyceride aggregation in cyclohexane exhibits a critical micellization concentration, *cmc*, showing a *cmc* can exist even in a system following open association. However, the *cmc* is associated with a change in balance with oligomeric and larger aggregates in the solution, not an onset of aggregate formation. It is demonstrated that reverse micelles can form in the absence of water stabilized by intersurfactant hydrogen bonds alone, and that the polarity and hydrogen bonding capability of triolein systematically reduces surfactant aggregation in comparison to cyclohexane. A comparison between CHARMM27 and CHARMM36 simulation models reveals that while trends are preserved, the models differ in quantitative prediction. Finally, consolidation of the general aggregation response trends predicted by the modelling are obtained via 7,7,8,8-tetracyanoquinodimethane dye (TCNQ) solubilization experiments on the corresponding model plant oil systems. The findings provide guidelines for predicting and controlling surfactant aggregation response in organic solvents via tuning the solvent polarity and hydrogen bonding ability, and a critical assessment of simulation and aggregation models for surfactant systems in organic solvents.

Introduction

Reverse micellar systems formed in organic solvents by surfactant self-assembly offer a highly dynamic and tuneable platform for synthesis of nanomaterials, solubilization, and controlled extraction of impurity or product species. Their polar cores provide a solubilization environment for polar molecules in the organic, nonpolar solvents. This enables, e.g. enhanced protein separation and chemical synthesis in biotechnology[1,2], and provides isolated, well-confined nanoenvironments for aqueous reactions toward nanoparticle synthesis and mesostructure construction[2–5]. Additionally, interesting responses to additives, such as a macroscopic phase change from a freely running solution into a viscous organogel upon addition of a suitable primer molecule, e.g. water, inorganic salts, or bile acids, have been reported for reverse micellar systems[6]. Systems with such structure and viscosity changes could have applications in topical drug delivery and as industrial lubricants.

In aqueous solutions, micellization is represented by a closed equilibrium between freely dispersed surfactants S_1 and micelles of aggregation number g

$$gS_1 \rightleftharpoons S_g \tag{1}$$

This simple model leads to onset of aggregate formation, micellization, at a well-defined concentration known as the critical micellization concentration (*cmc*) and captures quite well the aggregation response in aqueous solutions. Experimentally, the onset of micellization in water solutions shows typically as sharp changes in solution properties, and surfactant aggregation in aqueous solutions is relatively well understood since many decades ago, see e.g. Refs. 7 and 8. In contrast, the self-assembly of surfactants in organic, apolar solvents remains relatively poorly understood. This is highlighted, e.g. by the discussions over the nature of the *cmc*[9] and the role of water in the reverse micellization process[10,11]. Even the basic mechanism of aggregation remains in many cases illusive[12].

Similar to aqueous solutions, some apolar solvent surfactant systems show sharp changes in solution properties at specific sur-

[a] Department of Chemistry and Materials Science, Aalto University, P.O. Box 16100, 00076 Aalto, Finland. E-mail: maria.sammalkorpi@aalto.fi
[b] Department of Bioproducts and Biotechnology, Aalto University, P.O. Box 11000, 00076 Aalto, Finland. Email: monika.osterberg@aalto.fi

† Electronic Supplementary Information (ESI) available: the ESI contains system compositions, discussion on equilibration, convergence and choice of cluster cutoff, simulated size distributions and photographs of experimental samples. See DOI: 10.1039/b000000x/

‡

factant concentrations[9,13–15], characteristic of *cmc*, but more typically in apolar solvents, the aggregate formation sets on more gradually over a range of concentration, and a transition may remain altogether absent, see Refs. 12,15 and 16. The low overall aggregation numbers and continuous increase of the aggregate size with concentration point toward stepwise growth of the aggregates

$$\begin{aligned} S_1 + S_1 &\rightleftharpoons S_2 \\ S_1 + S_2 &\rightleftharpoons S_3 \\ S_1 + S_3 &\rightleftharpoons S_4 \\ &\vdots \end{aligned} \tag{2}$$

In this so called open association or multiple equilibrium model, monomers S_1, dimers S_2, and aggregates of higher aggregation numbers S_i are assumed to coexist in the solution in thermal equilibrium. Aggregates grow and decrease in size by stepwise monomer additions or removals, which leads to the model predicting continuously varying solution properties, in accordance with experimental observations for many apolar solvent/surfactant systems. However, unlike Equation 1, it does not reproduce the sharp transition associated with a critical micellization concentration, see Figure 1.

Experimentally establishing the mechanism of surfactant association in organic solvents is restricted by several practical obstacles. First, the aggregate size distribution generally cannot be measured directly but instead it must be inferred from indirect measurements. Second, probe molecules used in certain techniques, e.g. dye solubilization or labels, can influence the association propensity by acting as nucleation sites or by otherwise disrupting the association[14,17,18] or molecular conformations[19]. Third, the presence of residual water and variations in water content in experiments make comparisons between different systems difficult as many reverse micellar systems exhibit considerable sensitivity to water[11,20,21]. Finally, impurities in especially nonionic surfactants can influence the system behaviour via introducing additional surface active components into the system[22].

In the present work, we target clarifying surfactant association in apolar solvent environment for a model set of surfactants consisting of monopalmitin, dipalmitin, and palmitic acid – all hydrolysis products of tripalmitin – via detailed molecular dynamics simulations, and corroborating experiments. Our model solvents of choice are cyclohexane and a model plant oil, i.e. a triglyceride solvent (triolein). Figure 2 shows the structures of the examined solvents and surfactants. Simulations are the main method of choice in the study because they allow complete control over the system composition and resolution down to the level of atoms in individual surfactants. The examined surfactants have applications as emulsifiers and structuring agents[23] in food and cosmetic industry, as well as, are an important feedstock for the manufacturing of, e.g. biodegradable surfactants[24]. Particularly this set of surfactants is chosen as it offers a convenient series of closely related molecules with similar tails but differing headgroups, which allows systematic probing of the effect of headgroup polarity. Cyclohexane models a generic apolar hydrocarbon solvent, commonly used as a carrier media and solvent in lipase catalyzed production of fatty acid esters, including monoglycerides and diglycerides[1]. Triolein is a surrogate for vegetable oil, i.e. the natural environment of monoglycerides, diglycerides, and free fatty acids. It also provides a slightly more polar environment than cyclohexane and enables comparison of the aggregation responses between the two different solvents and also assessing the role of solvent hydrogen bonding capability.

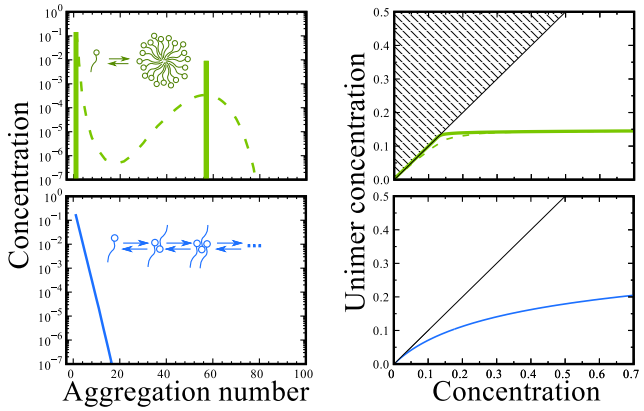

Fig. 1 Schematic view of aggregate size distributions (left panels) and the resulting concentration dependency of unimer concentration as predicted by closed association (green lines, Eq. 1) and open association (blue lines, Eq. 2)). Dashed lines correspond to typical aqueous aggregate size distribution, which the closed association model approximates. The boundary of the shaded region is set by unimer concentration equalling total concentration, i.e. the boundary shows the theoretical maximum unimer concentration.

Experimentally, the self-assembly of monoglycerides in nonpolar media has been studied extensively[15,22,25–32] in various hydrocarbon and triglyceride solvents but only a few works address aggregate formation of diglycerides and fatty acids[21,33–35]. Vapor pressure osmometry, calorimetry, light scattering, and small angle X-ray scattering (SAXS) studies indicate that small to medium sized reverse micelles of monoglycerides form in a wide range of hydrocarbon solvents[15,22,25–29]. The morphology of the aggregates can be controlled through temperature, solvent structure, and polar impurities[22,26,28,36]. In vegetable oils, monoglycerides can form inverse lamellar structures[30–32], which dissolve to form an isotropic fluid-like phase at a temperature dependent on the surfactant structure, concentration, and water content[30,31]. It is unclear what type of surfactant aggregates the isotropic phase is composed of, if any[33]. Contrary to monoglycerides, the aggregation of diglycerides and free fatty acids has been studied only in a few publications, and usually over a limited concentration range: both X-ray scattering[33] and dye solubilization[21,34,35] suggest that no diglyceride nor fatty acid aggregation takes place in oil solutions of up to 5 and 80 wt % of surfactant, respectively. These molecules may still form small aggregates in the oil: the experimental techniques have detection limits, or the aggregation could take place at a higher concentration.

An overwhelming majority of computational studies of reverse micellar systems have focused on the anionic Aerosol OT surfactant (sodium bis-(2-ethylhexyl)sulfosuccinate)[37–47]. In re-

cent years, however, there has been a surge of studies in which other surfactants and reverse micellar systems have been considered[21,48–60]. Due to time-scale challenges, many of these studies have focused on preassembled aggregates, their structure, and the structure of confined water, while the self-assembly process and the resulting aggregate size distribution have been characterized only in a very few publications, see Refs. 49,60–62.

Here, we assess the self-assembly characteristics of monopalmitin, dipalmitin and palmitic acid in triolein and cyclohexane in terms of hydrogen bonding ability, aggregate radii and size distribution. We extract aggregation energetics from the data, and investigate the nature of critical aggregation concentration in those systems that exhibit one. We assess critically the sensitivity of the self-assembly process to simulation model by comparing the predictions of two different versions of the CHARMM empirical force field, C27 and C36. As the findings indicate some discrepancy, 7,7,8,8-tetracyanoquinodimethane dye (TCNQ) solubilization characterization of the model plant oil system are performed to corroborate the findings. To our knowledge, this is the first micellization mechanism examination in organic solvents in which such an extented and systematically varying set of surfactants and solvents is examined. Additionally, the effect of force field on the size distribution and aggregation has not been explicitly addressed in prior studies of similar systems. The findings bear significance in understanding surfactant aggregation in organic solvents and provide means of engineering the response of surfactant-containing non-aqueous solutions.

Methods

Simulations. GROMACS 5.1.2 simulation package[63] with the all-atom empirical CHARMM36[64] and CHARMM27[65,66] lipid force fields were utilized for the molecular dynamics simulations. The CHARMM models are among the leading biomolecular force fields currently available and the two models compared in this article differ mainly in the degree of implicit polarization built into the partial charges of the ester moiety. Triolein molecular model was constructed based on dioleyl phosphatidylcholine by replacing the phosphorylcholine residue with an additional oleyl chain. The 1-palmitoyl glycerol (monopalmitin) and 1,2-dipalmitoyl glycerol (dipalmitin) models were constructed from dipalmitoyl phosphatidylglycerol parameters. Palmitic acid was constructed based on an acetic acid residue. The specific monopalmitin and dipalmitin isomers used in the simulations were chosen for no particular reason. The structure of the molecules and the abbreviations used for them in this work are shown in Figure 2.

Parrinello-Rahman barostat[67] ($P_{\mathrm{ref}} = 1$ bar, $\tau_{\mathrm{P}} = 2$ ps) and Bussi et al. thermostat[68] ($T_{\mathrm{ref}} = 70^{\circ}$C, $\tau_{\mathrm{T}} = 0.5$ ps) were utilized for pressure and temperature control of the simulations. The relatively high 70°C temperature was selected to speed-up diffusion in the apolar oil media, as well as, to ensure solubility of monopalmitin and dipalmitin. Electrostatic interactions were treated with the smooth Particle-Mesh Ewald scheme[69] (1.2 nm cutoff, ∼0.12 nm grid spacing, and 4th order interpolation). Lennard-Jones interactions were switched to zero between 1.0 nm and 1.2 nm. The recent buffered Verlet implementation was utilized for neighbour searching[70]. Leap-frog integrator with a 2 fs timestep was utilized to propagate the system configuration in time. Bonds involving hydrogens were constrained with the LINCS[71] algorithm.

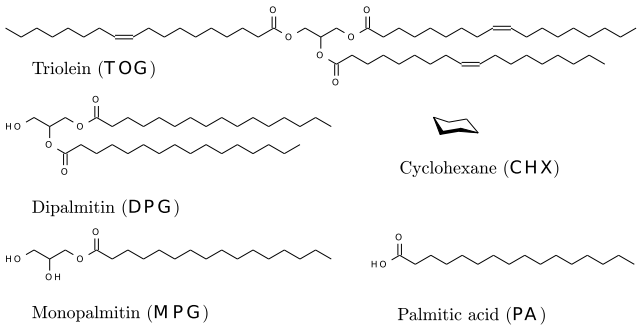

Fig. 2 Molecular structures of the surfactants and solvents utilized in this study. The abbreviations used throughout this work are given in parenthesis.

The starting configurations of the simulations were constructed by first placing the surfactant molecules in random orientations and locations in a vacuum box. For simulations with cyclohexane as the solvent, the box was filled with equilibrated bulk solvent, followed by the removal of overlapping solvent molecules. Although standard for small molecule solvents, this scheme produces poor configurations when the solvent molecules are large, like triolein. Hence, for the simulations with triolein as the solvent, the dispersed surfactants were brought into equilibrated bulk triolein by performing a brief, 50 ps λ-coupling simulation, in which the interactions between the surfactants and the solvent molecules were smoothly turned on. To prevent numerical instabilities from overlapping particles, soft-core interactions as implemented in GROMACS were utilized.

Systems with up to 30 wt-% surfactant (or 200 molecules) and $(10\ \mathrm{nm})^3$ in size were simulated. Production simulations were 200 ns long and the configurations were saved every 20 ps. The presented results correspond to an average over the last 175 ns of simulation trajectory. The 25 ns equilibration time for the systems was determined by following the convergence of free surfactant concentration and aggregate size distribution. Supplementary Information contains the complete list of simulated system compositions and sizes, as well as, the additional equilibration details.

In the analysis, an aggregate is defined as a group of surfactants whose polar headgroups are within a cut-off distance of 0.33 nm from the headgroup of at least one other surfactant in the group. The cut-off distance was determined by matching the generated size distributions to visual analysis of a handful of representative configurations at the higher end of the studied concentration range. Error of the size distribution was estimated based on the standard deviation of block averages.

Theory. Let us consider a surfactant system with free surfactant molecules S_1 and surfactant aggregates S_g where g is the aggregation number. In equilibrium, the chemical potential of a free surfactant molecule μ_1 is equal to the average chemical potential of a surfactant in aggregate μ_g/g, i.e. $g\mu_1 = \mu_g$, for all aggrega-

tion numbers g. This relation leads to the well-known aggregate size distribution

$$c_g = c_1^g \frac{\gamma_1^g}{\gamma_g} \exp\left(\frac{-g\Delta\mu_g^\circ}{RT}\right) \quad (3)$$

Here c_g is the concentration of aggregates of size g, $\Delta\mu_g^\circ$ is the difference in the standard chemical potentials for a free surfactant and the aggregate of size g, i.e. association free energy of aggregates of size g at infinite dilution. The activity coefficients of free surfactant molecule and aggregates of size g are γ_1 and γ_g, correspondingly. As usual, R is the molar gas constant and T temperature. In dilute solutions, the activity coefficients can be taken as $\gamma \approx 1$. Now, the $\Delta\mu_g^\circ$ profile can be solved based on, for example, the size distribution from simulations or the functional forms resulting from established micellization thermodynamics, such as the closed or open association models, Equations 1 and 2.

Here, the $\Delta\mu_g^\circ$ profile is solved based on the open association model, Equation 2; aggregate distributions from molecular modelling commonly present significant statistical noise and are thus not used directly for the $\Delta\mu_g^\circ$ profile. The choice also simplifies the interpretation of the findings in terms of the aggregation mode as deviations from the open association model, if present, are directly visible.

An equilibrium constant K_g for each step in the step-wise association process of Equation 2 can be written as

$$K_g = \frac{[S_{g+1}]}{[S_1][S_g]} = \frac{c_{g+1}}{c_1 c_g}. \quad (4)$$

In the most simple, classical formulation, K is assumed to be equal for all steps. A constant K leads to exponential size distribution $c_g = c_1^g K^{g-1}$. Plugging this into Equation 3 and solving for $\Delta\mu_g^\circ$ yields

$$\frac{\Delta\mu_g^\circ}{RT} = (g^{-1} - 1)\ln K. \quad (5)$$

This solution, however, is limited due to the assumption of constant K. For example, it cannot reproduce *cmc* as aggregates of increasing size are always present even at low concentration. Let us next assume that $\Delta\mu_g^\circ$ takes the form of an open association model but with two unique association steps after which energetically equivalent steps follow, i.e.

$$\frac{\Delta\mu_g^\circ}{RT} = \begin{cases} (g^{-1} - 1)\ln K_2 & g < 3 \\ -g^{-1}\ln K_2 K_3 K^{g-3} & g \geqslant 3 \end{cases} \quad (6)$$

where K_2 and K_3 are the dimerization and trimerization equilibrium constants, and K the equilibrium constant of subsequent association steps. The equilibrium constants can be converted to free energies of association following

$$\Delta G = RT \ln K. \quad (7)$$

So far, the treatment has omitted the activity coefficients γ in Equation 3. In concentrated systems, the activity coefficients cannot be neglected. As the concentration and size dependency of the activity coefficients is unclear in the current system, we follow the semi-empirical approach of Desplat and Care[72] in which size-dependent activity coefficients are replaced with a single average activity coefficient, i.e. $\gamma_1(c_{tot}) \approx \gamma_g(c_{tot}) = \bar{\gamma}(c_{tot})$. The concentration dependence of $\bar{\gamma}(c_{tot})$ is approximated using the Taylor expansion of $\ln\bar{\gamma}$, $\ln\bar{\gamma} \approx a c_{tot}$. Here a is a fitted constant. This treatment has been successfully applied to regular micelles[72], and the approach can be expected to perform adequately also for the present systems.

In fitting Equation 7 to the molecular simulations distributions, the relation of aggregate concentrations c_g and the total surfactant concentration c_{tot} is needed:

$$c_{tot} = \sum_{g=1}^{\infty} g c_g. \quad (8)$$

In the general case, the above sum is evaluated numerically up to a large enough g to cover the aggregates present in the solution. Here, the optimization is done using the Powell optimization algorithm, and the summation is truncated to include only the first 120 terms.

The presence of a *cmc* was examined via an extrapolation scheme that mimics osmometric determination of *cmc*. For this, Equation 3 is fit to the simulated size distributions to obtain the association energy $\Delta\mu_g^\circ$ for all aggregate sizes. The obtained $\Delta\mu_g^\circ$ allows aggregate size distribution to be calculated at any concentration and the distribution enables deriving expectation values for experimental observables such as the number-average aggregation number N_g. A *cmc* shows as a break in the slope of the N_g vs. c_{tot} curve. The *cmc* was numerically determined from the position of maximum in the second derivative of N_g with respect to surfactant concentration (N_g'' vs. c_{tot}).

To compare the distribution present in the simulations with the absorption response in the experiment, a means to estimate the absorption of TCNQ based on the aggregate size distribution is needed. If we assume, that the dye only solubilizes inside aggregates of a certain minimum size, and that at saturation the mean number of TCNQ molecules per aggregate, $\bar{n}$, is independent of surfactant concentration, the absorbance A can be crudely estimated from the size distribution as

$$A = \varepsilon d \bar{n} \sum_{g=N_{min}}^{\infty} c_g \quad (9)$$

where ε is the absorptivity of TCNQ, d is the path length, and N_{min} is the minimum aggregation number for dye solubilization. Parameters N_{min} and $\bar{n}$ cannot be resolved from the simulations, and are therefore fitted to experimental absorption data. This model presented by Equation 9 presents a direct, albeit coarse, means of comparing the simulated size distribution with the experimentally measured absorption response.

Experiments. Food grade rapeseed oil (Euro shopper, Bordeaux, France), monoglyceride (Danisco, Copenhagen, Denmark), diglyceride (Bachem, Babendorf, Switzerland) and 7,7,8,8-tetracyanoquinodimethane (Sigma-Aldrich, Missouri, USA) were used without further purification. Rapeseed oil acting as the solvent consisted of 97.1 wt % triglycerides, 0.6 wt % free fatty acids and less than 0.6 ppm phosphorus. Monoglyceride consisted of 97.1 % monoglycerides, 2.6 % diglycerides, 0.2

% triglycerides, and other minor impurities. The fatty acid composition was 36.3 wt % palmitic acid, 33.0 wt % oleic acid 8.4 wt % linoleic acid, 4.0 wt % stearic acid, as well as other minor fatty acid components. The diglyceride was composed of 99.7 % 1,2-dipalmitoyl-rac-glycerol, 0.2 % other monoglycerides and less than 0.1 % triglycerides.

Prior to use, all lipid material was dried. Rapeseed oil was dried overnight at 40°C by adding 3 % (w/w) 3 Å molecular sieves (Sigma-Aldrich). Monoglyceride and diglyceride were dried in a vacuum desiccator at room temperature using silica granules (Merck). Moisture contents of all the lipid material were determined using Karl-Fisher titration (Mettler-Toledo Titrator DL38). The moisture content of the vegetable oil was 0.015 wt-%, while the monoglyceride and diglyceride solutions contained $0.015-0.037$ wt-% and $0.015-0.12$ wt-% water, respectively, with the precise moisture content depending on surfactant concentration in the sample. Above 0.1 wt-% surfactant concentration the moisture levels correspond to molar water-to-surfactant ratio well smaller than one, suggesting that the systems can be considered practically water-free[31]. Below 0.1 wt-% the residual moisture in the solvent and the low surfactant concentration causes rapid increase of the water-to-surfactant ratio.

7,7,8,8-tetracyanoquinodimethane (TCNQ) dye solubilization technique[73,74] was used to determine the critical micellization concentration of monoglyceride and diglyceride in rapeseed oil. The method works by detecting light absorption from surfactant-dye charge-transfer complexes, which are postulated to form inside reverse micelles. Samples containing different concentrations of surfactant were prepared by diluting stock solutions with pure rapeseed oil. The TCNQ dye (1 mg / 1 g sample) was added, followed by 5 hours of agitation (70°C). Excess dye was sedimented by centrifugation (Heraeus Megafuge 1.0) at 40°C (the maximum temperature of the apparatus). To prevent the samples from cooling, the centrifugation time was decreased to 5 min and force increased to 2000 G in comparison to Kanamoto et al. procedure[74]. After centrifugation, the absorbance spectra of the supernatant was measured at 70°C using a UV spectrophotometer (Shimadzu UV-1800).

Results

The self-assembly occurring in solutions of monoglyceride, diglyceride, and fatty acid in organic solvents is characterized by simulations of monopalmitin, dipalmitin and palmitic acid at varying concentrations in model apolar solvent (cyclohexane) and model plant oil solvent (triolein). All examined systems show tendency towards surfactant self-aggregation. Figure 3 shows representative snapshots of the aggregates formed in the examined systems, their mean sizes and the principal axes lengths of ellipsoids fitted to the aggregates. The aggregates formed in both triolein and cyclohexane are highly dynamic, i.e. constantly form and break: monopalmitin in cyclohexane is the only system forming well-defined and persistent reverse micelles. In the other systems, the aggregates are mainly surfactant oligomers but occasionally transient larger aggregates form, and break. Visual analysis of the snapshots reveals that even the larger aggregates do not have a well-shielded polar core, a traditional characteristics of a reverse micelle, but instead are filamentous in shape or form lace-like threads. Typically, one axis of the ellipsoid fitted to the aggregates is much longer than the other two indicating axial elongation.

The exponential decay of the aggregate size distribution data of Figure 4 shows that in triolein the aggregate formation follows closely the classical open association model. In triolein, the first and second association steps deviate slightly from classical open association model while for monopalmitin, the deviation persists throughout the size distribution in simulations with the C27 force field but not by using the C36 force field. The deviation indicates that a population of larger monopalmitin reverse micelles could exist in triolein, but with low aggregate concentration. In comparison to triolein, in cyclohexane the distributions vary more: palmitic acid and dipalmitin exhibit an energetically unique dimerization step which is followed by regular open association response for the subsequent aggregation steps (exponential decay after clear deviation at first aggregation steps). Monopalmitin aggregate size distribution, on the other hand, is broad and clearly nonexponential in its decay. The response signifies that monopalmitin aggregates into well-defined reverse micelles in cyclohexane.

To quantify the aggregation propensities of each surfactant from the simulations, Figure 5 presents the calculated free surfactant (unimer) concentration as a function of total surfactant concentration. The data reveals that the aggregation propensity of the surfactants is smaller in triolein than in cyclohexane. Additionally, the outcome of the C36 and C27 force fields disagree to some extent. The smaller aggregation propensity in triolein is likely due to the higher polarity and hydrogen bonding capability of triolein, and the difference in force field predictions is discussed later in this article.

In Figure 5, the free surfactant concentration of palmitic acid grows monotonously in both solvents with increasing total surfactant concentration but for monopalmitin and dipalmitin the free surfactant concentration saturates to a constant level. Such plateauing is characteristic to micellization rather than open association – this observation is seemingly at odds with the size distributions following exponential decay in triolein. The discrepancy could be explained by 1) nonideal effects due to, e.g. interaggregate interactions, which are known to decrease the free surfactant concentration in concentrated solutions[72,75] or by 2) weakly oligomerizing systems exhibiting *cmc*-like behaviour provided that the first association step is less favourable than subsequent association steps, as proposed based on theoretical calculations in Ref. 76. Our data contains support for both explanations: the first aggregation step of monopalmitin and dipalmitin are typically slightly less favoured than the following steps and the aggregation energies calculated based on the size distributions depend on surfactant concentration – a possible sign of nonideality (data provided in Figure S3 in Supplementary Information).

Let us next assess the presence of *cmc* in the systems, as described in Methods. Table 1 lists the results of fitting Equation 3 to the simulated size distributions while Figures S5-S6 compare the fit with the actual size distributions (see Figure 4 for a subset of the data). Generally, the fit quality is good even for large aggregation numbers and the concentration dependency in the size

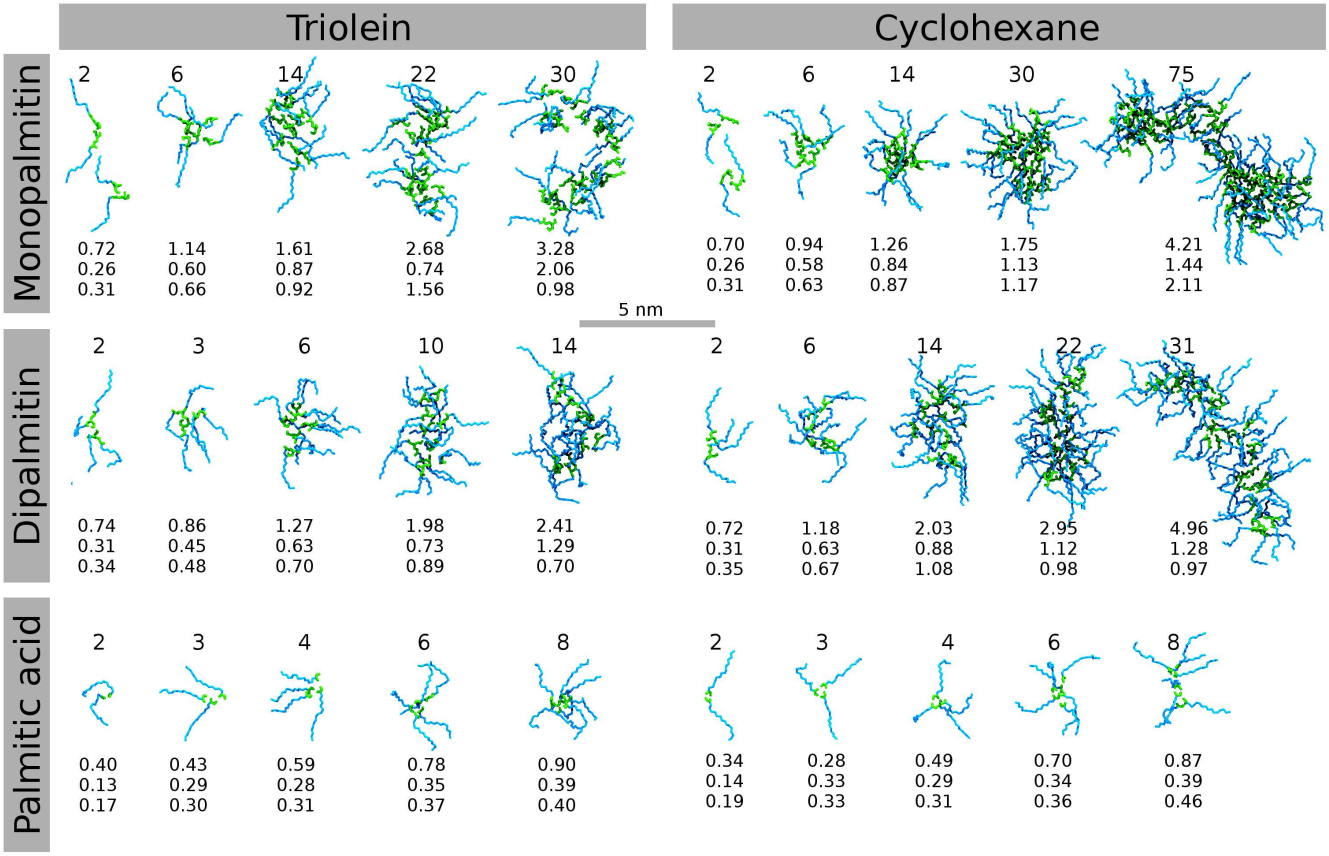

Fig. 3 Simulation snapshots of monopalmitin, dipalmitin, and palmitic acid aggregates formed in triolein and cyclohexane. For each cluster, the number above indicates the aggregation number while the three numbers below show the average semiaxis lengths of an ellipsoid matching the polar core size (headgroups) in nanometers. Surfactant headgroups are colored green and tails blue, respectively. All snapshots are to scale (see scalebar).

distributions is accurately captured. Table 1 shows by the positive ΔG values that in triolein, surfactant aggregation is energetically disfavoured (palmitic acid) or just barely favoured (dipalmitin and monopalmitin) while in cyclohexane all three species present a negative free energy of aggregation ΔG indicating preference to aggregate.

It is worth noting that the activity factors a in Table 1, obtained by the fit procedure show relatively large scatter in value. This could indicate that the term also compensates for simulation related artefacts such as slightly wrong cluster cutoff or finite-size effects in addition to correcting for nonidealities in aggregation response. However, tests on the effect of system size and the cluster size sensitivity analysis presented in SI show that neither the cluster cutoff choice or finite size effects are particularly prevalent. Because the activity factors a could also be compensating for the simulation model, no physical meaning is given to the values of a, and instead it is treated as a generic correction parameter.

Figure 6 presents the average aggregation numbers calculated from the simulations (symbols) and from the fitted size distributions (lines). In triolein, all examined surfactants show monotonous growth of the average aggregate size with increasing surfactant concentration, and simulated aggregate sizes follow closely exponential growth. This means that no *cmc* can be identified for these systems. However, in cyclohexane the average aggregate size initially grows fast but eventually reaches a constant value with increasing surfactant concentration for dipalmitin and palmitic acid. Monopalmitin is an exception as its mean aggregate size first shows an initial lag period before starting to increase fast with increasing concentration. Such inflection point between the slow and fast aggregate size growth regions is commonly interpreted as an operational *cmc*, which was determined to be 14 mM for both C27 and C36 force fields for monopalmitin. Although the two force fields capture a virtually identical *cmc* value for monopalmitin, the sharpness of the inflection point (as judged from the magnitude of $N_g''(c_{tot})$ at *cmc*) was eight times higher in the simulations by the C27 in comparison those by the C36 force field. This difference between the force fields in the inflection point sharpness presumably reflects the larger difference between propensity of oligomeric and micellar aggregates in the simulations using C27 force field.

Before moving to more detailed analysis of the modelling results, it is instructive to assess if and how the transient, thread-like aggregates predicted by the modelling manifest in real solvent systems in experiments, and if verification for the simulational findings can be obtained from experiments. For cyclohexane the presence of 1-mono-olein *cmc*, in agreement with the observations, has been previously established[15]. However, as the aggregation of monoglycerides and diglycerides in triolein has been

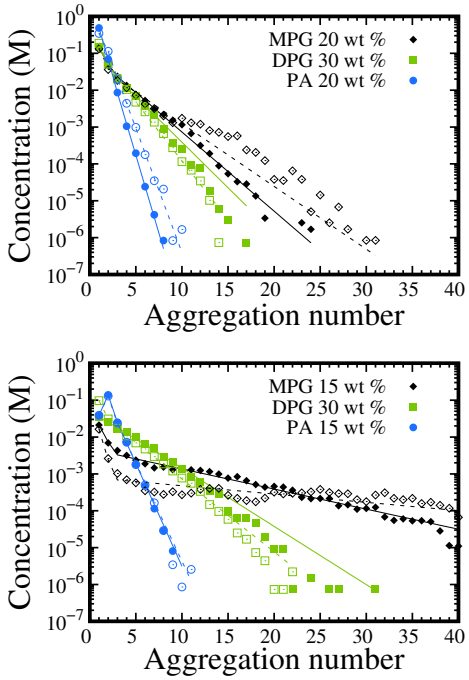

Fig. 4 Aggregate size distributions in triolein (top panel) and cyclohexane (bottom panel). Filled and open symbols correspond to data calculated using C36 and C27 force fields, respectively, while solid and dashed lines show the corresponding fit to Equations 3 and 6. Purely exponential decay (straight line) means open association model is valid for the system, whereas curviness indicates micellization. For visual clarity, only the most concentrated systems are presented. The more dilute systems follow closer the exponential decay in their aggregate size distribution and the decay becomes steeper with decreasing total surfactant concentration.

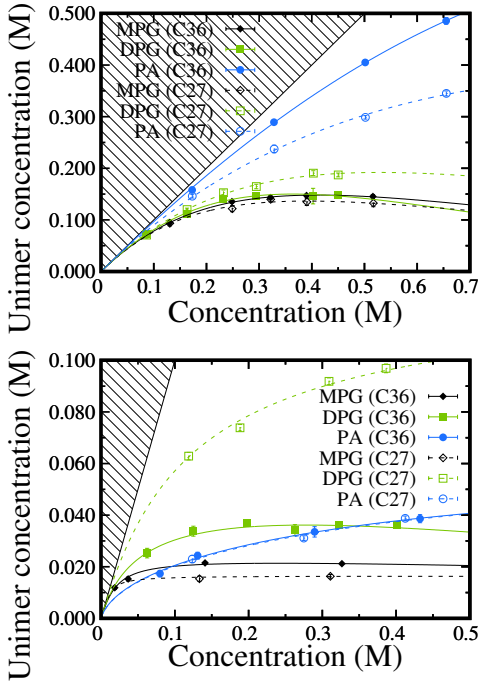

Fig. 5 Free surfactant (unimer) concentration as a function of total surfactant concentration in triolein (top panel) and cyclohexane (bottom panel). Filled symbols correspond to simulation using the C36 force field and open symbols to the C27 force field. Black, blue and green lines represent the fit of Equation 3 to the data.

characterized in prior experimental studies only over a limited concentration range[33,34], we investigated their aggregation response via experiments using the widely used TCNQ solubilization method[73,74]. The absorbance of TCNQ, see Figure 7, with varying amounts of dispersed monoglyceride changed abruptly at 10 wt-% ($\sim$ 250 mM) concentration. This suggests aggregation or some form of surfactant-dye interaction is taking place at elevated concentrations of monoglyceride. We note, however, that the samples lack the bright color change associated with TCNQ complexes, suggesting that the change in absorbance could also result from the intensive color of monoglyceride that affects the absorbance at these very high concentrations. The photographs of the experimental samples showing the colors of the samples are presented in the Supplementary Information as Figure S4. Diglyceride samples, on the other hand, do not show substantial changes in the absorbance data nor in visual appearance, suggesting lack of diglyceride aggregates in vegetable oils. Our previous work[21] contains data for the aggregation response of fatty acids in the same oil system: no aggregation, even at surfactant concentrations as high as 80 wt% is observed. In total, the TCNQ data on the monoglyceride and diglyceride addition can be interpreted so that aggregation in the diglyceride-vegetable oil system is insignificant over the studied concentration range but for monoglyceride some aggregation may take place.

If the increase in monoglyceride absorbance results from monoglyceride aggregation, i.e. corresponds to presence of an apparent *cmc*, the monoglyceride experiments are seemingly at odds with the simulation results in Figure 5 which suggests a lack of *cmc*. However, the surfactant-TCNQ complexation takes place only inside reverse micelles, not in the presence of freely dispersed surfactants. This suggests the technique can not detect aggregates that are smaller than some minimum detection size limit - unlike e.g. vapor pressure osmometry. To investigate if this bias to detect only the larger aggregates can explain the discrepancy between the experiments and simulations, i.e. absence of abrupt changes in the aggregate size distribution in the simulations, the absorbance response of TCNQ was estimated from simulated size distributions using the simplified model presented by Equation 9. Figure 7 shows the comparison of the experimentally measured absorbance, and that calculated from the simulated distribution assuming that dye solubilization (complexation) takes place only in aggregates that are larger than 4-5 surfactants in size. The data shows that the characteristics of the experimental absorbance data of monoglycerides can be reproduced to a very good match from the simulated size distributions. This suggests that TCNQ absorbance data which shows potentially an onset of aggregation can plausibly result from the TCNQ being subject to detecting aggregates larger than some limiting size while the analysis of the simulation size distribution counts all, even small oligomeric aggregates, and predicts a continuously evolving size distribution. This means, that the differences rise from the method of detection, rather than from major differences in

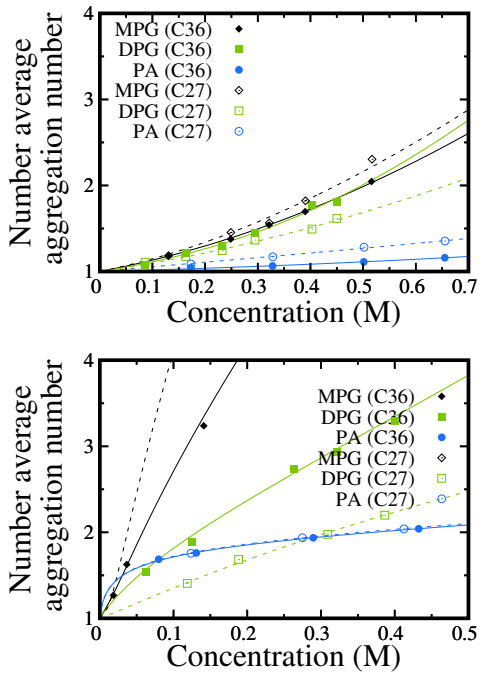

Fig. 6 Average aggregation numbers in triolein (top panel) and cyclohexane (bottom panel) as a function of surfactant concentration calculated from the simulations. The symbols correspond to simulated data and the lines are the corresponding fit to Equation 3.

the underlying experimental and simulational size distributions. Curiously, the simulated dipalmitin systems also show increasing absorbance at elevated concentrations. This indicates that the aggregation propensity of dipalmitin - particularly in the case of the C36 force field - may be overestimated in comparison to monopalmitin. Obviously, the approach presented by Equation 9 for deriving the expected absorbance response from the simulated size distribution is rather crude here, but it demonstrates how differing detection limits could explain the discrepancy in the evolution of experimental absorbance data and simulational number-average aggregation numbers.

To characterize the interactions driving the observed aggregation response in the simulations, Figure 8 presents the mean number of surfactant-solvent, surfactant-surfactant, and surfactant intramolecular hydrogen bonds normalized per surfactant in triolein and cyclohexane. Hydrogen bonding is analyzed here as association of surfactants in oil is mainly driven by polar interactions between the surfactant headgroups. In cyclohexane, no solute-solvent hydrogen bonds are possible, but each triolein molecule contains three ester groups that are capable of accepting hydrogen bonds from hydroxyl or carboxylic acid groups of the surfactants. The data shows that in triolein surfactant-triolein hydrogen bonds are replaced by surfactant-surfactant hydrogen bonds following an almost linear dependency on the surfactant concentration. Intramolecular hydrogen bonding, on the other hand, appears insensitive to surfactant concentration. In contrast to this, in cyclohexane both intermolecular and intramolecular hydrogen bonding show clearly non-linear concentration dependence. This difference arises from the lower polarity of cyclohexane and the lack of hydrogen bonding capability of the solvent.

Table 1 Association energies of dimerization ΔG_2, trimerization ΔG_3, and subsequent steps ΔG, as well as the activity factor a, calculated based on fitting Equation 3 to the simulated size distributions of the surfactants palmitic acid (PA), dipalmitin (DPG), and monopalmitin (MPG) in solvents triolein (TOG) and cyclohexane (CHX). The energies of association relate to equilibrium constants via Equation 7.

Surf.	Solv.	Model	ΔG_2 ($\frac{\text{kJ}}{\text{mol}}$)	ΔG_3 ($\frac{\text{kJ}}{\text{mol}}$)	ΔG ($\frac{\text{kJ}}{\text{mol}}$)	a (M^{-1})
PA	TOG	C36	5.10	5.50	5.08	0.424
PA	TOG	C27	1.68	3.35	2.95	0.421
DPG	TOG	C36	0.09	-0.64	-1.43	0.945
DPG	TOG	C27	0.32	-0.70	-1.26	0.540
MPG	TOG	C36	-0.50	-1.39	-2.14	0.667
MPG	TOG	C27	-0.74	-1.84	-2.92	0.587
PA	CHX	C36	-12.46	-3.95	-5.17	0.177
PA	CHX	C27	-12.55	-4.11	-5.51	0.136
DPG	CHX	C36	-7.34	-7.52	-7.33	0.519
DPG	CHX	C27	-3.46	-4.98	-5.35	0.015
MPG	CHX	C36	-7.61	-8.36	-10.29	0.186
MPG	CHX	C27	-6.22	-8.13	-11.54	0.033

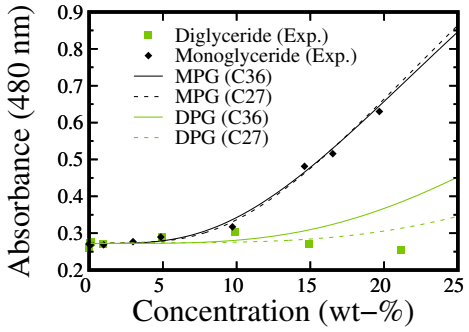

Fig. 7 Comparison of the experimental absorbance of monoglyceride and diglyceride in vegetable oil at 480 nm after TCNQ solubilization and the estimates calculated from the simulated size distributions. The water-to-lipid molar ratio of 10 wt-% monoglyceride and diglyceride samples were 0.05 and 0.21, respectively. Straight and dashed lines correspond to scaled absorbances calculated based on the simulated size distributions using Equation 9.

While the hydrogen bonding data in Figure 8 shows similar general trends for systems described within the C27 and C36 force fields, the two models result in significantly differing prediction for the absolute numbers of formed hydrogen bonds. In triolein, the C36 force field results in $16-144$ % higher values for the number of solvent-surfactant hydrogen bonds than the C27 force field. Interestingly, the surfactant-surfactant hydrogen bonding responds differently to the change of force field for the three studied surfactants: For monopalmitin and palmitic acid, intramolecular hydrogen bonding is reduced and surfactant aggregation enhanced with the C27 force field description in comparison to description with the C36 force field. However, with dipalmitin, the C36 force field reduces the number of intermolecular surfactant-surfactant hydrogen bonds and increases significantly intramolecular bonding (by $77-79$ %) in comparison to C27 force field.

Inspection of the simulation trajectories suggests that this difference in force field response between monopalmitin and dipalmitin is due to the hydroxyl-carbonyl group arrangement of

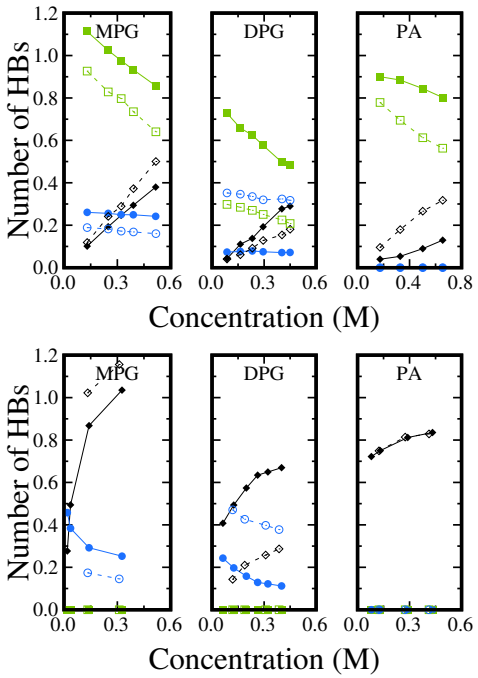

Fig. 8 Mean number of hydrogen bonds per surfactant in triolein (top panel) and cyclohexane (bottom panel). Intermolecular surfactant-solvent hydrogen bonds are shown in green, surfactant-surfactant hydrogen bonds in black, and intramolecular surfactant-surfactant hydrogen bonds in blue. Open symbols and dashed lines represent C27 results, while filled symbols and unbroken lines C36.

dipalmitin being optimal for the formation of intramolecular hydrogen bonds. Additionally, the lack of a second hydroxyl group connected to the same chain reduces the pulling and pushing the hydrogen bonds experience which enhances their lifetime, and proportionally also the mean number of hydrogen bonds.

Figure 9 shows the distribution of surfactant-surfactant hydrogen bonds formed to different types of acceptor oxygens. The data shows that the fraction of number of hydrogen bonds formed between hydroxyl groups and ester group oxygens and the number of hydrogen bonds between two hydroxyl groups is somewhat sensitive to the force field employed. Specifically, C27 model predicts a higher fraction of hydroxyl-hydroxyl hydrogen bonds for monopalmitin and dipalmitin than C36. While this difference could result from changes in either hydroxyl or ester group parameters in the two models, the data in Figure 8 for palmitic acid suggests that the force field dependence of the hydrogen bonding, and by extension the differences in the resulting size distributions in Figure 4, originate particularly from the differences in ester group parametrization between C27 and C36. The isolation of the cause to a single functional group, and its parametrization, demonstrates the importance of force field validation.

Discussion

In this paper, the aggregation of monopalmitin, dipalmitin and palmitic acid in triolein and cyclohexane solvents was examined by molecular dynamics simulations. Additionally, TCNQ dye solubilization experiments were conducted using vegetable oil as the solvent. In the simulations, all three surfactant species

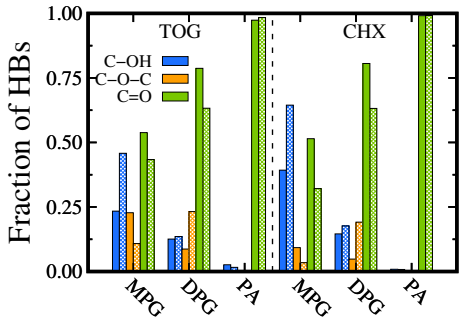

Fig. 9 Fraction of hydrogen bonds formed to each type of acceptor oxygen in a surfactant in triolein (right) and cyclohexane (left). Solid bars correspond to the C36 force field and patterned bars to the C27 force field results. The data corresponds to simulations closest to 320 mM surfactant concentration.

were found to self-aggregate in both solvents but the aggregation propensity was much weaker in triolein. The formed aggregates in both solvents were predominantly small clusters composed of only a few molecules, with the exception of monopalmitin forming also thread-like, weak aggregates in triolein and spherical and elongated reverse micelles in cyclohexane. The aggregate size distributions and system response to increase in surfactant concentration were found to match a modified open association model. The model predicted absence of *cmc* for all systems except monopalmitin in cyclohexane. In total, the findings show that also relatively weakly polar surfactants can form reverse micelles in apolar solvents without water to support the formation of a polar core. However, for surfactant aggregation in the absence of water, the hydrogen bonding capability of the surfactants is in key role – a minimum of two hydrogen bonding groups (monoglyceride) was needed here for the emergence of larger surfactant aggregates. The findings provide understanding on surfactant aggregation in organic solvents, but also on how to choose surfactants and solvents for desired aggregation response.

In the current work, only monopalmitin in cyclohexane system formed clear aggregates and had a *cmc* of 14 mM based on numerical fitting. Previously, Konno et al.[15] have reported that the *cmc* of 1-monoolein varied between 4.2 mM and 8.3 mM in the temperature range $30-50$ °C. A simple extrapolation based on these values yields an estimate of 12 mM for the *cmc* in 70°C – in reasonable agreement with our simulation estimate of 14 mM for 1-monopalmitin considering the differences in system composition and uncertainties associated with experimental and computational determination of *cmc*. Further confidence in the simulation results is provided by the apparent aggregation numbers reported by Konno et al. matching closely those shown in Figure 6. The aggregation numbers of monocaprin (at 30°C), as reported by Debye and Coll[26], are likewise in good agreement with the current findings; however, their measured concentration range is extremely narrow. Finally, Shrestha et al.[28] investigated monomyristin/cyclohexane system (5 wt %, 70°C) with SAXS and found the aggregates to be prolate ellipsoids with maximum dimensions of 2.8 nm. While exact comparison is difficult due to the slightly different surfactants and because their samples contain

unknown levels of moisture, the formation of prolate aggregates is in qualitative agreement with our results. Hence, considering the existing literature data, both employed simulation models, C27 and C36, seem to perform with almost quantitative accuracy in capturing the monoglyceride/cyclohexane system aggregation response as function of the surfactant concentration.

Even though the term *cmc* is used here, the aggregation response phenomenon in the monopalmitin/cyclohexane system is somewhat distinct from the critical micellization concentration in aqueous systems. Namely, in aqueous systems the *cmc* marks the onset of micellization yet in the organic solvents of our work large aggregates are present in significant quantity only at concentrations exceeding several times the apparent *cmc*. As discussed in length by Nyrkova and Semenov[76], the answer to this discrepancy lies in the shape of the aggregate size distribution: The first few association steps here are always slightly less favourable than subsequent steps. This effectively splits the distribution into two populations, oligomeric and micellar, which compete for dominance over solution properties. At low surfactant concentration, the contribution of the micellar population is negligible but with increasing surfactant concentration, micelles become the dominant species because of the lower energy of the micellar aggregates and the greater width of the micellar population. The sharpness of the resulting transition depends on the energy difference between the oligomers and micellar aggregates, as illustrated by the differences in C27 and C36 size distributions and aggregation numbers. This means that the apparent *cmc*s observed here mark the onset of the solution properties being dominated by aggregates from the micellar population; the apparent *cmc* in these systems does not correspond to the onset of aggregation or formation of larger reverse micelles as such.

A significant debate whether the formation of large reverse micelles is possible without the presence of, at least trace amounts of, water persists in the literature. Recently, the topic has been investigated mostly computationally – with mixed results. Atomistic simulations of Bradley-Shaw et al.[48] resulted in spontaneous formation of monoolein reverse micelles in anhydrous heptane and toluene while Khoshnood and Abbas[77] suggested on the basis of coarse-grained simulations and thermodynamic modeling that a polar impurity is necessary for initiating aggregation. Our simulation results are in line with Bradley-Shaw et al. and show that the hydrogen bonding capacity of two hydroxyl groups is enough to trigger the formation of large reverse micelles in cyclohexane – even at the relatively high temperature of 70°C. However, one hydroxyl group in the surfactant (such as found in dipalmitin and palmitic acid) appears to be insufficient to cause aggregation beyond oligomerization. The aggregation propensity is also influenced by the structure and number of hydrocarbon moieties which affect both the surfactant solubility and micelle formation due to steric effects. Here, the aggregates were very small and thus steric hindrance probably did not affect micelle formation. However, no *cmc* was detected for palmitic acid (having one hydrocarbon tail) suggesting that indeed the head group structure is the dominating factor in the examined systems. In total, the observations suggest that nonionic surfactants with intrinsically weak hydrogen bonding donor capabilities may require water to initiate reverse micellization, while surfactants with sufficient hydrogen bonding power in the headgroup do not.

Interestingly, replacing cyclohexane with a solvent containing hydrogen bonding sites appears to prevent the formation of large aggregates, even for those surfactants that have two hydroxyl groups per surfactant (monopalmitin). Actually, this mirrors the findings of Debye and coworkers[22,26] who investigated the aggregation tendency and hydrogen bonding of monoglycerides in benzene, carbon tetrachloride and chloroform. They found evidence of aggregation and intermolecular hydrogen bonding in benzene and carbon tetrachloride but not in chloroform[22,26]. This suggests that the hydrogen bonding capabilities of the slightly polar C-H bond in chloroform[78] serve a similar role to the ester groups in our triolein solvent. It should be noted that the surfactant aggregation propensity is also slightly altered by solvents incapable of forming hydrogen bonds[26,29,48,77]. This is presumably due to differences in solvent polarity and surfactant tail - solvent mixing energy. Our work in which a model organic solvent without hydrogen bonding capability (cyclohexane) and triolein solvent were compared systematically, however, suggests that the hydrogen bonding capacity of the solvent is in a key position at attenuating or enhancing reverse micellization in systems driven by surfactant-to-surfactant hydrogen bonding.

We observed significant differences in, e.g. the aggregation propensities of monopalmitin and in the hydrogen bonding patterns between predictions by the C27 and C36 force fields. In prior simulational studies of reverse micellar systems, the force field dependency of the results has typically not been addressed explicitly despite several reports suggesting force fields as an important factor in accuracy of reverse micellar descriptions[38,54]. As discussed earlier, both the experimental literature and our own experiments provide confidence in the simulation results. However, given the assumptions and simplifications required to complete the comparison of the simulational distribution and the experimental absorbance in Figure 7, the data here and the existing literature data do not quite enable discerning which of the two examined models is more accurate. However, inspection of the differences in the C27 and C36 lipid models reveals that in the update of the older C27 force field, major changes were made in the ester linkage. Both the partial charges and the van der Waals parameters were modified, and the dihedrals refitted accordingly with the purpose of alleviating the underestimation of the gel-to-liquid transition temperature of lipid bilayers in aqueous environment that the C27 force field is subject to[64]. Specifically, in C36 the hydration free energy of the ester moiety, -20.3 kJ/mol, was intentionally overestimated in comparison to experimental value, -13.9 kJ/mol. This implicit polarization enables more accurate reproduction of the lipid bilayer response in aqueous solvent but may not be so accurate in an organic solvent environment. Indeed, the hydrogen bonding data in Figures 8 and 9 suggests that the C36 force field favours hydrogen bonding to ester groups which results in diminished aggregation propensity due to solvent competition and looser micelle packing.

While implicit polarization may be necessary to capture the response of lipids and related species in aqueous bilayers, the old C27 force field with all its short comings may actually rep-

resent interactions in the present anhydrous and apolar systems more accurately, as the charges are closer to unpolarized vacuum charges. Consequently the predictions of the C27 force field in this work are more plausible to be the ones closer to actuality in the modelling here. While the C27 force field may still be slightly off, the performance it demonstrates for cyclohexane in terms of *cmc*, average aggregation number and aggregate shape suggests that the predicted size distributions in triolein are at least qualitatively correct. We note, however, that the C36 force field might be more appropriate for reverse micellar lipid simulations with large amounts of water.

Conclusions

We have investigated the self-assembly behaviour of monopalmitin, dipalmitin and palmitic acid in anhydrous cyclohexane and triolein. The results show moderate oligomerization in all systems, non-traditional thread-like aggregates for monoglyceride in model vegetable oil (triolein), while large reverse micelles and an apparent critical micellization concentration were found for monopalmitin in cyclohexane. Contrary to aqueous systems, the apparent *cmc* was found to correspond to a smooth transition from oligomers to larger aggregates – the finding highlights that concepts or models used in aqueous micellization are not directly, as such, transferable to micellization in organic solvents. The findings of this work suggest that a modified open association model is a more appropriate approach to describing the present systems, and similar systems, than the classical open or closed association models which are traditionally used for predicting surfactant aggregation.

Comparative simulations using CHARMM27 and CHARMM36 lipid models showed qualitative agreement but relatively large deviations, which were traced to differences in ester group polarization. In particular, CHARMM36 force field involves an implicit polarization contribution, which enables more accurate description of lipid bilayers in aqueous solvent but is perhaps less accurate in an organic solvent which screens much less the charges. The presence of reverse micelles in cyclohexane but not in triolein insinuate that aggregation can be switched off by introducing hydrogen bonding sites to the solvent. Additionally, the result implies that water is not strictly necessary for nonionic reverse micellization provided that the headgroup is sufficiently polar for the solvent. The findings enable engineering surfactant-apolar solvent systems such as emulsions and gels via the hydrogen bonding capability, i.e. surfactant and solvent choice, and provide tools for improved understanding of biological surfactant aggregation in organic media for biotechnology, drug delivery, alimentary uses, and chemical engineering processes.

Conflicts of interest

There are no conflicts to declare.

Acknowledgements

The authors thank Laura Tiittanen and Dr. Robertus Nugroho for aid with the experimental work, and Dr. Tuula Lehtimaa and Dr. Susanna Kuitunen for useful discussions. This work was a part of the Academy of Finland's Flagship Programme under Projects No. 318890 and 318891 (Competence Center for Materials Bioeconomy, CERES). The work has been supported by Aalto University School of Chemical Engineering doctoral programme (S.V.), Academy of Finland and the Finnish Funding Agency for Innovation. Computational resources by CSC IT Centre for Science, Finland, and RAMI – RawMatTERS Finland Infrastructure are also gratefully acknowledged.

Notes and references

1 H. Stamatis, A. Xenakis and F. Kolisis, *Biotechnol. Adv.*, 1999, **17**, 293 – 318.

2 R. S. Chaurasiya and H. U. Hebbar, *Nanoscience in Food and Agriculture 4*, Springer International Publishing, Cham, Switzerland, 2017, pp. 181–211.

3 S. Xu, H. Zhou, J. Xu and Y. Li, *Langmuir*, 2002, **18**, 10503–10504.

4 L. Qi, J. Ma, H. Cheng and Z. Zhao, *J. Phys. Chem. B*, 1997, **101**, 3460–3463.

5 H. Shi, L. Qi, J. Ma and H. Cheng, *Chem. Commun.*, 2002, 1704–1705.

6 G. Palazzo, *Soft Matter*, 2013, **9**, 10668–10677.

7 R. Nagarajan, *Surfactant Science and Technology: Retrospects and Prospects*, CRC Press, Boca Raton, Florida, US, 2014, ch. 1, pp. 3–52.

8 H. Wennerström and B. Lindman, *Phys. Rep.*, 1979, **52**, 1 – 86.

9 G. N. Smith, P. Brown, S. E. Rogers and J. Eastoe, *Langmuir*, 2013, **29**, 3252–3258.

10 H. F. Eicke and H. Christen, *Helv. Chim. Acta*, 1978, **61**, 2258–2263.

11 Z. J. Yu, N. F. Zhou and R. D. Neuman, *Langmuir*, 1992, **8**, 1885–1888.

12 L. Klíčová, P. Šebej, P. Štacko, S. K. Filippov, A. Bogomolova, M. Padilla and P. Klán, *Langmuir*, 2012, **28**, 15185–15192.

13 E. L. Michor and J. C. Berg, *Langmuir*, 2015, **31**, 9602–9607.

14 Y.-C. Jean and H. J. Ache, *J. Am. Chem. Soc.*, 1978, **100**, 6320–6327.

15 K. Kon-No, T. Jin-No and A. Kitahara, *J. Colloid Interface Sci.*, 1974, **49**, 383 – 389.

16 H. Gutmann and A. Kertes, *J. Colloid Interface Sci.*, 1975, **51**, 406 – 411.

17 J. Lang, G. Mascolo, R. Zana and P. L. Luisi, *J. Phys. Chem.*, 1990, **94**, 3069–3074.

18 B. Baruah, L. A. Swafford, D. C. Crans and N. E. Levinger, *J. Phys. Chem. B*, 2008, **112**, 10158–10164.

19 M. Sammalkorpi and T. Lazaridis, *Biophys. J.*, 2007, **92**, 10 – 22.

20 R. Scartazzini and P. L. Luisi, *J. Phys. Chem.*, 1988, **92**, 829–833.

21 O.-P. Lehtinen, R. W. N. Nugroho, T. Lehtimaa, S. Vierros, P. Hiekkataipale, J. Ruokolainen, M. Sammalkorpi and M. Österberg, *Colloids Surf. B*, 2017, **160**, 355 – 363.

22 P. Debye and W. Prins, *J. Colloid Sci.*, 1958, **13**, 86 – 98.

23 A. P. B. Ribeiro, M. H. Masuchi, E. K. Miyasaki, M. A. F.

Domingues, V. L. Z. Stroppa, G. M. de Oliveira and T. G. Kieckbusch, *J. Food Sci. Technol.*, 2015, **52**, 3925–3946.

24 S. Martin, *Surfactants from Renewable Resources*, Wiley-Blackwell, Chichester, West Sussex, UK, 2010, ch. 1, pp. 1–19.

25 J. Jagur-Grodzinski, R. Frame and R. M. Izatt, *J. Colloid Interface Sci.*, 1985, **105**, 73 – 79.

26 P. Debye and H. Coll, *J. Colloid Sci.*, 1962, **17**, 220 – 230.

27 L. K. Shrestha, R. G. Shrestha, M. Abe and K. Ariga, *Soft Matter*, 2011, **7**, 10017–10024.

28 L. K. Shrestha, O. Glatter and K. Aramaki, *J. Phys. Chem. B*, 2009, **113**, 6290–6298.

29 L. K. Shrestha, T. Sato, D. P. Acharya, T. Iwanaga, K. Aramaki and H. Kunieda, *J. Phys. Chem. B*, 2006, **110**, 12266–12273.

30 A. López-Martínez, J. Morales-Rueda, E. Dibildox-Alvarado, M. Charó-Alonso, A. Marangoni and J. Toro-Vazquez, *Food Res. Int.*, 2014, **64**, 946 – 957.

31 C. H. Chen and E. M. Terentjev, *Langmuir*, 2009, **25**, 6717–6724.

32 T. Gulik-Krzywicki and K. Larsson, *Chem. Phys. Lipids*, 1984, **35**, 127 – 132.

33 Y. Li, A. S. Fabiano-Tixier, K. Ruiz, A. R. Castera, P. Bauduin, O. Diat and F. Chemat, *Food Chem.*, 2015, **173**, 873 – 880.

34 B. Chen, D. J. McClements and E. A. Decker, *Food Chem.*, 2014, **142**, 365 – 372.

35 K. Kittipongpittaya, A. Panya, D. J. McClements and E. A. Decker, *J. Am. Oil Chem. Soc.*, 2014, **91**, 453–462.

36 L. K. Shrestha, R. G. Shrestha, K. Aramaki, J. P. Hill and K. Ariga, *Colloids Surf. A*, 2012, **414**, 140 – 150.

37 A. V. Nevidimov and V. F. Razumov, *Mol. Phys.*, 2009, **107**, 2169–2180.

38 A. V. Martinez, L. Dominguez, E. Małolepsza, A. Moser, Z. Ziegler and J. E. Straub, *J. Phys. Chem. B*, 2013, **117**, 7345–7351.

39 S. Abel, F. Sterpone, S. Bandyopadhyay and M. Marchi, *J. Phys. Chem. B*, 2004, **108**, 19458–19466.

40 S. Abel, M. Waks, M. Marchi and W. Urbach, *Langmuir*, 2006, **22**, 9112–9120.

41 J. Tian and A. E. García, *J. Chem. Phys.*, 2011, **134**, 225101.

42 M. H. H. Pomata, D. Laria, M. S. Skaf and M. D. Elola, *J. Chem. Phys.*, 2008, **129**, 244503.

43 J. Chowdhary and B. M. Ladanyi, *J. Phys. Chem. B*, 2009, **113**, 15029–15039.

44 G. Mudzhikova and E. Brodskaya, *Colloid J.*, 2006, **68**, 738–742.

45 E. N. Brodskaya and G. V. Mudzhikova, *Mol. Phys.*, 2006, **104**, 3635–3643.

46 G. Mudzhikova and E. Brodskaya, *Colloid J.*, 2006, **68**, 729–737.

47 V. R. Vasquez, B. C. Williams and O. A. Graeve, *J. Phys. Chem. B*, 2011, **115**, 2979–2987.

48 J. L. Bradley-Shaw, P. J. Camp, P. J. Dowding and K. Lewtas, *J. Phys. Chem. B*, 2015, **119**, 4321–4331.

49 P. de la Iglesia, V. W. Jaeger, Y. Xi, J. Pfaendtner and L. D. Pozzo, *Langmuir*, 2015, **31**, 9006–9016.

50 A. J. Mills, J. Wilkie and M. M. Britton, *J. Phys. Chem. B*, 2014, **118**, 10767–10775.

51 L. Klíčová, E. Muchová, P. Šebej, P. Slavíček and P. Klán, *Langmuir*, 2015, **31**, 8284–8293.

52 F. M. Agazzi, N. M. Correa and J. Rodriguez, *Langmuir*, 2014, **30**, 9643–9653.

53 B. Fuglestad, K. Gupta, A. J. Wand and K. A. Sharp, *Langmuir*, 2016, **32**, 1674–1684.

54 S. Vierros and M. Sammalkorpi, *J. Chem. Phys.*, 2015, **142**, 094902.

55 S. Vierros and M. Sammalkorpi, *Phys. Chem. Chem. Phys.*, 2015, **17**, 14951–14960.

56 S. Abel, N. Galamba, E. Karakas, M. Marchi, W. H. Thompson and D. Laage, *Langmuir*, 2016, **32**, 10610–10620.

57 M. Mannoor, S. Kang and Y. K. Suh, *Adv. Cond. Matter Phys.*, 2015, **2015**, 739458.

58 R. Gordon, S. T. Stober and C. F. Abrams, *J. Phys. Chem. B*, 2016, **120**, 7164–7173.

59 B. Qiao, T. Demars, M. Olvera de la Cruz and R. J. Ellis, *J. Phys. Chem. Lett.*, 2014, **5**, 1440–1444.

60 M. Wang, T. Fang, P. Wang, X. Tang, B. Sun, J. Zhang and B. Liu, *Soft Matter*, 2016, **12**, 8177–8185.

61 L. Lu and M. L. Berkowitz, *J. Am. Chem. Soc.*, 2004, **126**, 10254–10255.

62 M. Marchi and S. Abel, *J. Phys. Chem. Lett.*, 2015, **6**, 170–174.

63 M. J. Abraham, T. Murtola, R. Schulz, S. Páll, J. C. Smith, B. Hess and E. Lindahl, *SoftwareX*, 2015, **1-2**, 19 – 25.

64 J. B. Klauda, R. M. Venable, J. A. Freites, J. W. O'Connor, D. J. Tobias, C. Mondragon-Ramirez, I. Vorobyov, A. D. MacKerell and R. W. Pastor, *J. Phys. Chem. B*, 2010, **114**, 7830–7843.

65 S. E. Feller and A. D. MacKerell, *J. Phys. Chem. B*, 2000, **104**, 7510–7515.

66 P. Bjelkmar, P. Larsson, M. A. Cuendet, B. Hess and E. Lindahl, *J. Chem. Theory Comput.*, 2010, **6**, 459–466.

67 M. Parrinello and A. Rahman, *J. Appl. Phys.*, 1981, **52**, 7182–7190.

68 G. Bussi, D. Donadio and M. Parrinello, *J. Chem. Phys.*, 2007, **126**, 014101.

69 U. Essmann, L. Perera, M. L. Berkowitz, T. Darden, H. Lee and L. G. Pedersen, *J. Chem. Phys.*, 1995, **103**, 8577–8593.

70 S. Páll and B. Hess, *Comput. Phys. Commun.*, 2013, **184**, 2641 – 2650.

71 B. Hess, H. Bekker, H. J. C. Berendsen and J. G. E. M. Fraaije, *J. Comput. Chem.*, 1997, **18**, 1463–1472.

72 J.-C. Desplat and C. Care, *Mol. Phys.*, 1996, **87**, 441–453.

73 S. Muto, Y. Shimazaki and K. Meguro, *J. Colloid Interface Sci.*, 1974, **49**, 173 – 176.

74 R. Kanamoto, Y. Wada, G. Miyajima and M. Kito, *J. Am. Oil Chem. Soc.*, 1981, **58**, 1050–1053.

75 F. K. von Gottberg, K. A. Smith and T. A. Hatton, *J. Chem. Phys.*, 1997, **106**, 9850–9857.

76 I. A. Nyrkova and A. N. Semenov, *Eur. Phys. J. E*, 2005, **17**, 327–337.

77 A. Khoshnood and A. Firoozabadi, *Langmuir*, 2015, **31**, 5982–5991.

78 N. Goutev and H. Matsuura, *J. Phys. Chem. A*, 2001, **105**, 4741–4748.